

Short-range aggregation regulation of conjugated polymers: high mobility and cyclic tensile stability driven by chemical crosslinking

Rui Chen^{1,2}, Yiting Liu^{1,2}, Teng Li¹, Zhongxiang Peng¹, Hongxiang Li⁵, Sichao Huang^{1,2}, Zicheng Ding^{4*}, Xiaozheng Duan^{1*}, Yuan-Qiu-Qiang Yi^{3*} and Yanchun Han^{1,2*}

¹State Key Laboratory of Polymer Science and Technology, Changchun Institute of Applied Chemistry, Chinese Academy of Sciences, Changchun 130022, China

²School of Applied Chemistry and Engineering, University of Science and Technology of China, Hefei 230026, China

³Printable Electronics Research Center, Nano Devices and Materials Division, Suzhou Institute of Nano-Tech and Nano-Bionics, Chinese Academy of Sciences, Suzhou 215123, China

⁴Shaanxi Engineering Laboratory for Advanced Energy Technology, School of Materials Science and Engineering, Shaanxi Normal University, Xi'an 710119, China

⁵College of Polymer Science and Engineering, State Key Laboratory of Polymer Materials Engineering, Sichuan University, Chengdu 610065, China

E-mail: zcding@snnu.edu.cn (Zicheng Ding)

xzduan@ciac.ac.cn (Xiaozheng Duan)

yqqyi2020@sinano.ac.cn (Yuan-Qiu-Qiang Yi)

ychan@ciac.ac.cn (Yanchun Han)

* To whom correspondence should be addressed

The Supporting Information includes:

1 Experimental section

Figure S1. The synthetic route of the BP crosslinker.

2 Supplementary data

Figure S2. ^1H NMR of BP.

Figure S3. ^{13}C NMR of BP.

Table S1. The thicknesses of different IDTBT films.

Figure S4. GISAXS images and corresponding one-dimensional curves were obtained by integrating in-plane direction for the three types of films.

Figure S5. Contact angles of water and diiodomethane on IDTBT and BP.

Table S2. Detailed information on the crystallographic parameters of different IDTBT films was obtained by one-dimensional XRD curves.

Table S3. Detailed information on the surface energy of IDTBT and BP was obtained from contact angle experiments.

Figure S6. Typical polarized UV-vis absorption spectra of different IDTBT films under strain.

Figure S7. Detailed information on the crystallographic parameters of different IDTBT films under strain was obtained by one-dimensional XRD curves (In-plane).

Table S4. Detailed information on the crystallographic parameters of different IDTBT films under strain was obtained by one-dimensional XRD curves.

Table S5. The thickness of different IDTBT films after 100% strain.

Figure S8. AFM height images of (a) pristine and (b) 2% IDTBT films under 100% strain.

Figure S9. Coarse-grained model of an IDTBT polymer (with the backbone in red and sidechains in blue) and a BP molecule (in yellow and green).

Molecular dynamics simulation

Table S6. The elastic modulus and fracture strain of pristine, 1%, 2% and 3% films. The data were obtained from five samples.

Figure S10. The transfer curves of the OFET devices fabricated from different IDTBT films (pristine, 1%, 2%, and 3%) under different strains (25%, 50%, 75%, and 100%). The stretching direction is parallel to the direction of charge carrier transport between the source and drain electrodes.

Figure S11. The transfer curves of the OFET devices fabricated from different IDTBT films (pristine, 1%, 2%, and 3%) under different strains (25%, 50%, 75%, and 100%). The stretching direction is perpendicular to the direction of charge carrier transport between the source and drain electrodes.

Figure S12. Transfer curves of OFET devices prepared after cyclic stretching of different films at 30% strain. The stretching direction is perpendicular to the direction of charge carrier transport between the source and drain electrodes.

Figure S13. Transfer curves of OFET devices prepared after cyclic stretching of different films at 30% strain. The stretching direction is parallel to the direction of charge carrier transport between the source and drain electrodes.

Figure S14. Changes in carrier mobility after uniaxial (left) and cyclic stretching

(right).

Table S7. BGTC OFET parameters of different IDTBT films: Each set of saturation mobility (μ_{sat}) (both the average and maximum), threshold voltage (V_{th}), and $I_{\text{on}}/I_{\text{off}}$ ratio data were extracted from five transistors with $L = 200 \mu\text{m}$ and $W = 1000 \mu\text{m}$ (parallel direction for uniaxial stretching and perpendicular direction for cyclic stretching).

Table S8. BGTC OFET parameters of different IDTBT films: Each set of saturation mobility (μ_{sat}) (both the average and maximum), threshold voltage (V_{th}), and $I_{\text{on}}/I_{\text{off}}$ ratio data were extracted from five transistors with $L = 200 \mu\text{m}$ and $W = 1000 \mu\text{m}$ (perpendicular direction for uniaxial stretching and parallel direction for cyclic stretching).

Table S9. Charge mobilities of IDTBT films under strain in the previous literature.

3 References

1 Experimental Section

Materials. Chemical structures of IDTBT and BP are shown in Figure 1a.

IDTBT with a weight-average molecular weight of 205 kg mol⁻¹ and a dispersity of 2.16 was obtained from Textron Photonics Materials Technology Co., LTD. The polystyrene-block-poly(ethylene-ran-butylene)-block-polystyrene (SEBS, H1052) was obtained from Asahi Kase. Octadecyltrimethoxysilane (OTMS) and trichloroethylene were obtained from Sigma-Aldrich. Poly(dimethylsiloxane) (PDMS, Sylgard 184) with curing agents were obtained from Dow Corning. Chloroform (CF) and other solvents were purchased from Xilong Science Co., LTD. They were used as received without further processing.

The BP crosslinker was synthesized in our lab (**Figure S1**). Compounds A and B were purchased from Shanghai Leyan and used as received without any further purifications. Compound **A** (4.15 g, 21 mmol) and compound **B** (2.31 g, 10 mmol) were added to a round flask, followed by the addition of K₂CO₃ (4.14 g, 30 mmol). Dimethylformamide (DMF, 30 mL) was used as a reaction solvent. The mixture was vigorously stirred at 70 °C overnight. After cooling to room temperature, the mixture was poured into ice water and filtered. The filter was washed with water, hexane, and CH₃OH successively. Then, the filtered cake was purified by chromatography on silica gel as a white solid (4.01 g, 86% yield).

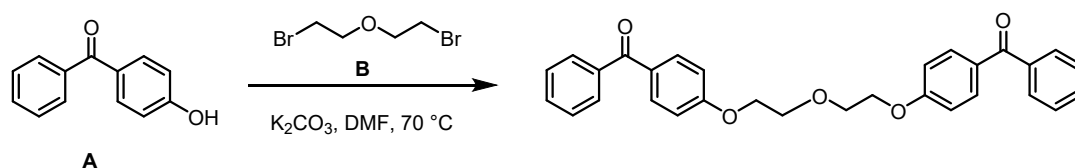


Figure S1. The synthetic route of the BP crosslinker.

Substrate Preparation. OTMS-modified SiO₂/Si substrates were prepared as follows¹: First, the 300-nm-SiO₂/Si wafers were sequentially washed with deionized water, acetone, and isopropanol. Afterward, the wafers were treated with piranha solution (H₂O₂:H₂SO₄=30:70, v/v) for 20 min and then exposed to UV/ozone for 25 min, respectively. The OTMS solution (0.26 mg mL⁻¹ in trichloroethylene) was then

cast onto the treated wafers. 40 μL OTMS solution was allowed to self-assemble for 10 s and then spin-coated at 3000 rpm for 30 s. Subsequently, the wafers were exposed to ammonia for 10 h, followed by cleaning with toluene and chloroform for use.

The SEBS-modified SiO_2/Si substrates were prepared as follows: SEBS was dissolved in toluene and heated at 90 $^\circ\text{C}$ for 8 h to give a homogeneous solution with a concentration of 20 mg mL^{-1} . The 300-nm- SiO_2/Si wafers were sequentially washed with deionized water, acetone, and isopropanol. Then, 70 μL SEBS solution was spun onto the cleaned SiO_2/Si wafers at 3000 rpm for 60 s. The thickness of the SEBS dielectric layer was about 1.3 μm (tested by Tencor P-7 Probe Profilometer).

The Crosslinked Film Preparation. The IDTBT polymers with various content of BP crosslinkers (0%, 1%, 2%, and 3% in weight) were dissolved in chloroform. The concentration of IDTBT polymer was 5 mg mL^{-1} . The solutions were stirred at 50 $^\circ\text{C}$ overnight, and then naturally cooled to room temperature before use. For film preparation, 50 μL IDTBT solutions were spin-coated onto the OTMS-modified SiO_2/Si substrates at 1000 rpm for 30 s. The films were irradiated under 365 nm UV light for 10 seconds (KM-160 LED UV curing chamber).

Morphology Characterization.

Fourier transform infrared spectroscopy (FTIR) was conducted using a Bruker ALPHA instrument in the range of 400-4000 cm^{-1} . Raman measurements were performed on a LabRam HR 800 laser confocal Raman spectrometer manufactured by HORIBA Jobin Yvon. The laser wavelength used was 532 nm and the exposure time was 5 s. The ultraviolet-visible (UV-Vis) absorption spectra were recorded using Lambda 750 spectrometer from Perkin-Elmer. The measurements were performed in the wavelength range of 350-1000 nm. The UV-Vis absorption spectra of the stretched film were tested as follows: The films were initially prepared on the OTMS-modified SiO_2/Si substrates. Subsequently, poly(dimethylsiloxane) (PDMS, $w_{\text{precursor}}: w_{\text{curing agents}} = 15:1$, heated at 70 $^\circ\text{C}$ for 12 h) was attached to the film surface and carefully peeled off to transfer the film onto the PDMS. Then, while stretching the film on a stretching instrument, the UV-Vis absorption test was carried out using an instrument equipped

with a polarizer. Two-dimensional grazing incidence wide-angle X-ray scattering (2D GIWAXS) test were completed at BL02U2, Shanghai Synchrotron Radiation Facility (SSRF). The X-ray incidence angle was set to 0.2° , and the X-ray wavelength (λ) used were 1.13 \AA . Data processing was performed using the GIWAXS-tools software. Sector integration was performed on the 2D GIWAXS images for the regions of $0\text{-}10^\circ$ and $80\text{-}90^\circ$ to obtain 1D XRD curves. Atomic force microscopy (AFM) was conducted using a Bruker Dimension ICON AFM at room temperature. The scanned area for imaging was $2 \times 2 \text{ \mu m}^2$. The polarizing microscopy (POM) was performed using a Zeiss Axio ImagerA2 equipped with two crossed polarizers. The films for POM tests were first prepared on the OTMS-modified SiO_2/Si substrates. Then, the films were stretched to the corresponding strains by PDMS (Sylgard 184, $w_{\text{PDMS}}: w_{\text{curing agents}} = 15:1$, heated at $70 \text{ }^\circ\text{C}$ for 12 h), and subsequently transferred onto the SEBS-modified SiO_2/Si substrates respectively for measurement.

Mechanical Characterization.

Film-on-Water Technique (FOW)²⁻³: First, $50 \text{ }\mu\text{L}$ different IDTBT solutions were spin-coated onto the clean glass slides at 1000 rpm for 30 s. The poly(dimethylsiloxane) (PDMS, Sylgard 184, Dow Corning) was prepared by mixing precursor with curing agents with a mass ratio of 10:1 and then heating at $70 \text{ }^\circ\text{C}$ for 12 h. After that, the cured PDMS was cut into the shape of a dog bone using a template. The length and width at the center of the PDMS were 5 and 3 mm, respectively. Next, it was covered on the surface of the polymer film. After oxygen plasma etching treatment for 3 min, the PDMS on the surface was gently peeled off, and a dog-bone-shaped polymer film was obtained. Then, the glass slide with the film was placed in hydrofluoric acid vapor for 15 s. It was made to gently touch the water surface so that the polymer film floated on the water surface. Finally, the floated film was fixed by two grips of a customized stretching machine and stretched at $1 \text{ mm}\cdot\text{min}^{-1}$ until the film fractured.

Film-on-Elastomer Technique (FOE)²: The crack-on-set (COS) strain of the films was determined using the FOE method. First, $50 \text{ }\mu\text{L}$ different IDTBT solutions were spin-coated onto the OTMS-modified SiO_2/Si substrates at 1000 rpm for 30 s. The

PDMS substrate was prepared by mixing precursor with curing agents with a mass ratio of 15:1 and heating at 70 °C for 12 h. After covering the PDMS onto the surface of IDTBT films, the PDMS substrates were then gently peeled off to complete the transfer. Then the IDTBT film adhered PDMS substrate was stretched to different strains at a rate of 24 mm min⁻¹ using a stretching table. The stretched films were finally transferred onto the SEBS-modified SiO₂/Si substrates to measure the crack-on-set strain by optical microscopy.

Electrical Characterization. Bottom gate/top contact (BGTC) organic field-effect transistor (OFET) devices ($L/W = 200 \mu\text{m}/1000 \mu\text{m}$) were utilized to investigate the electrical properties of the different IDTBT films. The gold was deposited under high vacuum conditions as the source and drain electrodes. The IDTBT films, which were initially deposited on OTMS-modified SiO₂/Si substrates, were adhered to PDMS elastomers ($w_{\text{PDMS}}: w_{\text{curing agents}} = 15:1$) and stretched to different strains. Subsequently, they were transferred onto SEBS-modified SiO₂/Si substrates. The OFET devices were tested in an air environment by a probe station connected to a Keysight B1500A semiconductor parameter analyzer, where both the output and transfer curves were obtained. The carrier mobility (μ_{sat}) was calculated from the transfer curve from the following equation:

$$\mu_{\text{sat}} = \left(\frac{\partial \sqrt{I_D}}{\partial V_G} \right)^2 (2L/WC_i) \quad (1)$$

where μ_{sat} is the carrier mobility, I_D is the drain-source current, V_G is the gate voltage, C_i (5 nF cm⁻²) is the capacitance per unit area of the dielectric in OFET device.

2 Supplementary data

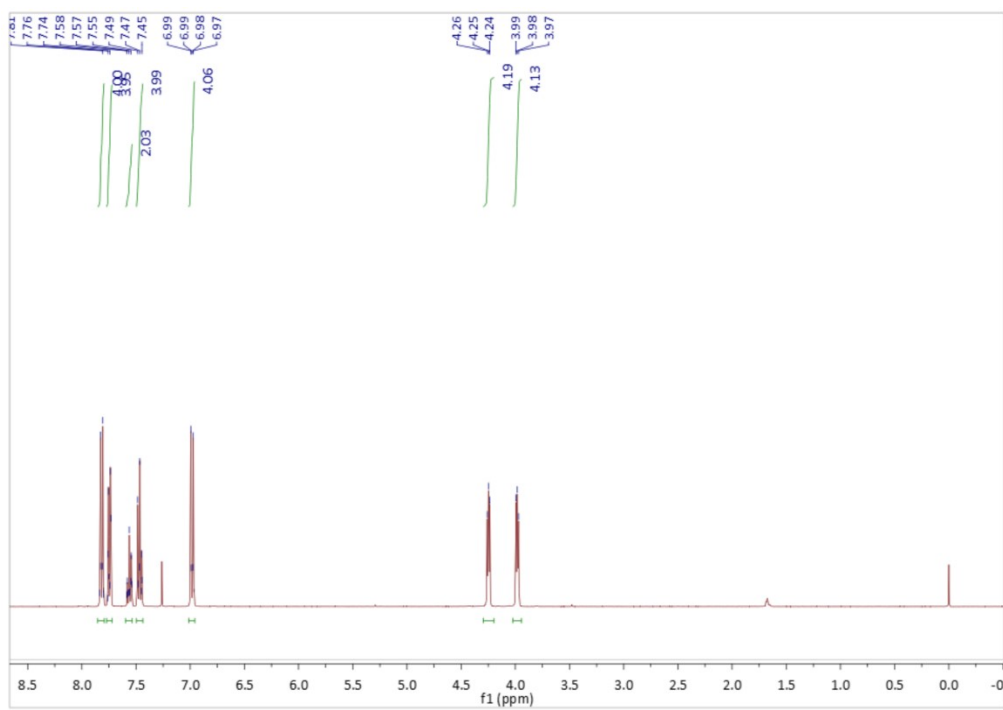


Figure S2. ¹H NMR of BP.

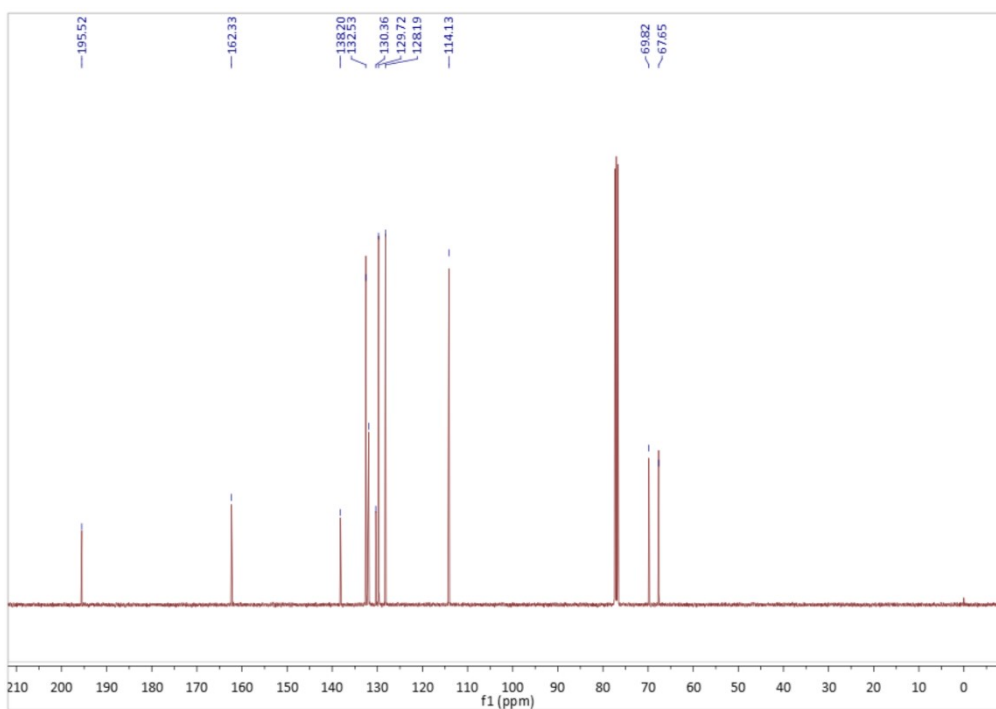


Figure S3. ^{13}C NMR of BP.**Table S1.** The thicknesses of different IDTBT films.

	Pristine	1%	2%	3%
1	83.7	88.5	86.1	86.5
2	92.6	90.9	88.6	84.2
3	97.5	84.0	90.3	88.9
4	92.7	92.1	84.7	83.0
5	86.2	85.2	88.8	88.7
	90.5 ± 5.5	88.1 ± 3.5	87.7 ± 2.3	86.3 ± 2.6

Table S2. Detailed information on the crystallographic parameters of different IDTBT films was obtained by one-dimensional XRD curves.

Film	$(100)^a$				$(010)^a$		$(001)^b$				$(010)^b$	
	q_z (\AA^{-1})	d (\AA)	FWHM (\AA^{-1})	CCL (\AA)	q_z (\AA^{-1})	d (\AA)	q_z (\AA^{-1})	d (\AA)	FWHM (\AA^{-1})	CCL (\AA)	q_z (\AA^{-1})	d (\AA)
Pristine	0.26	24.17	0.06	93.20	1.48	4.25	-	-	-	-	1.45	4.33
1%	0.26	24.17	0.06	93.20	1.48	4.25	0.41	15.32	0.04	139.80	1.45	4.33
2%	0.26	24.17	0.06	93.20	1.50	4.19	0.41	15.32	0.06	93.20	1.45	4.33
3%	0.26	24.17	0.06	93.20	1.50	4.19	-	-	-	-	1.45	4.33

 a : out-of-plane; b : in-plane

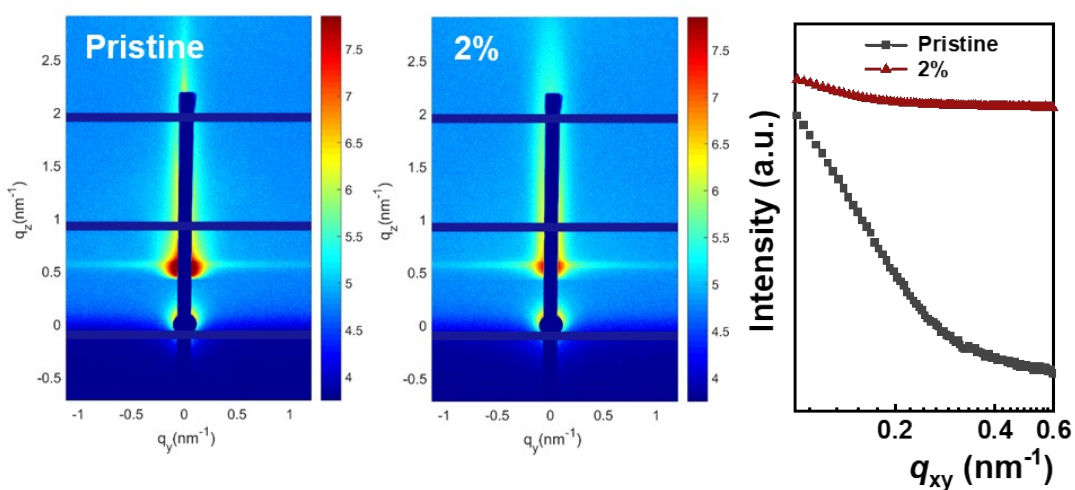


Figure S4. GISAXS images and corresponding one-dimensional curves were obtained by integrating in-plane direction for the three types of films.

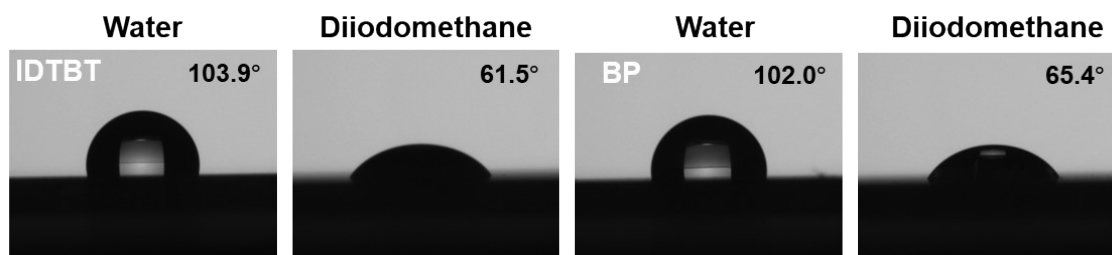


Figure S5. Contact angles of water and diiodomethane on IDTBT and BP.

Table S3. Detailed information on the surface energy of IDTBT and BP was obtained from contact angle experiments.

Material	θ ($^{\circ}$)		γ (mJ/m 2)		
	H $_2$ O	CH $_2$ I $_2$	γ_s^p	γ_s^d	γ_s
IDTBT	103.9	61.5	0.2	28.0	28.2
BP	102.0	65.4	0.6	24.9	25.5

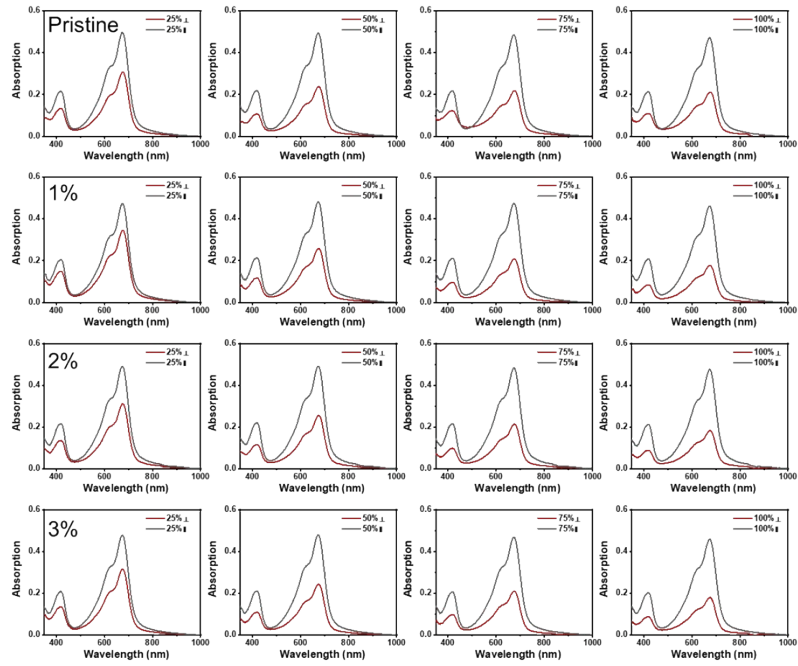


Figure S6. Typical polarized UV-vis absorption spectra of different IDTBT films under strain.

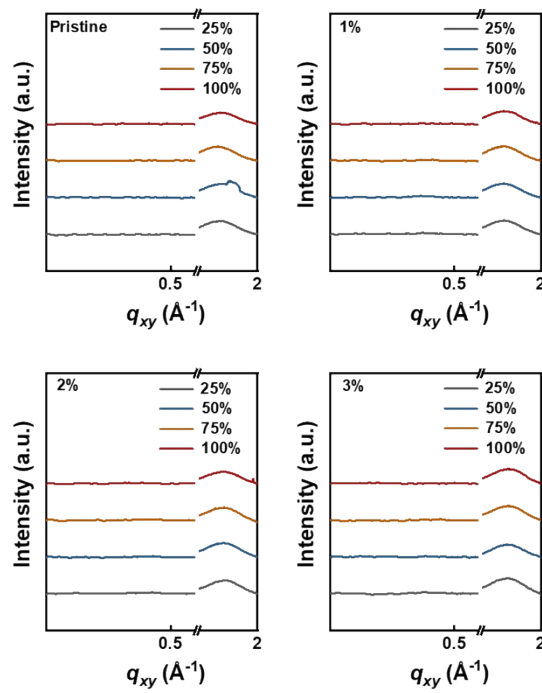


Figure S7. Detailed information on the crystallographic parameters of different IDTBT films under strain was obtained by one-dimensional XRD curves (In-plane).

Table S4. Detailed information on the crystallographic parameters of different IDTBT films under strain was obtained by one-dimensional XRD curves.

Film	Strain	(100) ^a				(010) ^a		(010) ^b	
		q_z (\AA^{-1})	d (\AA)	FWHM ($1/\text{\AA}$)	CCL (\AA)	q_z (\AA^{-1})	d (\AA)	q_{xy} (\AA^{-1})	d (\AA)
Pristine	25%	0.25	25.13	0.06	93.20	1.48	4.25	1.51	4.16
	50%	0.25	25.13	0.06	93.20	1.48	4.25	1.51	4.16
	75%	0.25	25.13	0.06	93.20	1.45	4.33	1.48	4.25
	100%	0.25	25.13	0.05	111.84	1.48	4.25	1.51	4.16
1%	25%	0.25	25.13	0.06	93.20	1.48	4.25	1.53	4.10
	50%	0.25	25.13	0.06	93.20	1.48	4.25	1.53	4.10
	75%	0.25	25.13	0.06	93.20	1.48	4.25	1.53	4.10
	100%	0.25	25.13	0.06	93.20	1.48	4.25	1.53	4.10
2%	25%	0.26	24.17	0.06	93.20	1.50	4.19	1.56	4.03
	50%	0.26	24.17	0.06	93.20	1.50	4.19	1.56	4.03
	75%	0.26	24.17	0.06	93.20	1.50	4.19	1.56	4.03
	100%	0.26	24.17	0.06	93.20	1.50	4.19	1.56	4.03
3%	25%	0.26	24.17	0.06	93.20	1.50	4.19	1.56	4.03
	50%	0.26	24.17	0.06	93.20	1.50	4.19	1.56	4.03
	75%	0.26	24.17	0.06	93.20	1.50	4.19	1.56	4.03
	100%	0.26	24.17	0.06	93.20	1.50	4.19	1.56	4.03

^a: Out-of-plane; ^b: In-plane

Table S5. The thickness of different IDTBT films after 100% strain.

	Pristine (100%)	1% (100%)	2% (100%)	3% (100%)
1	77.4	75.2	75.5	71.3
2	75.8	70.1	70.1	64.1
3	71.1	76.2	71.6	72.9
4	73.1	74.1	69.3	71.6
5	75.5	69.3	69.7	69.0
	74.6±2.5	72.9±3.1	71.2±2.5	69.8±3.5

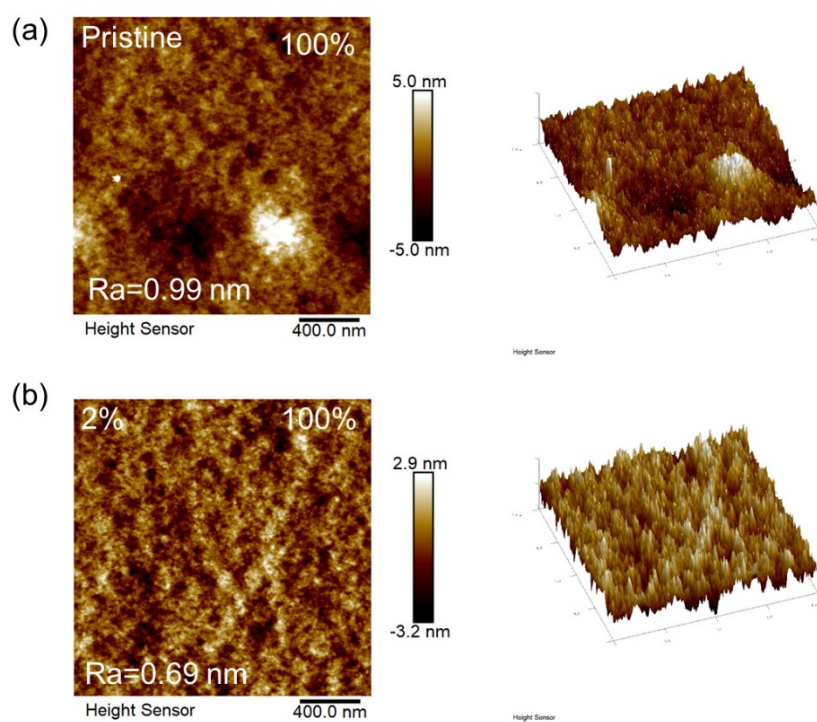


Figure S8. AFM height images of (a) pristine and (b) 2% IDTBT films under 100% strain.

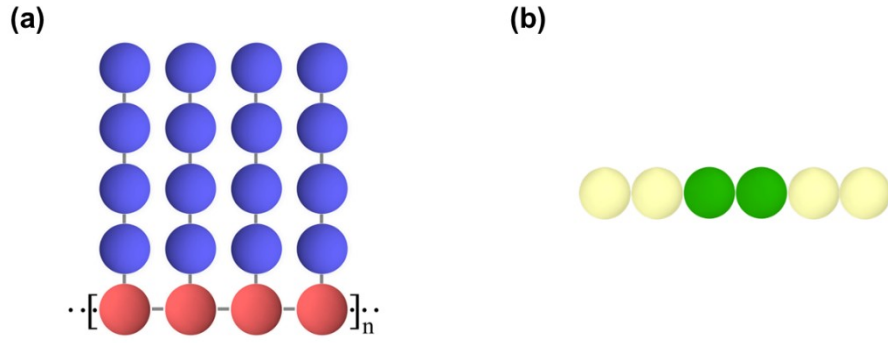


Figure S9. Coarse-grained model of an IDTBT polymer (with the backbone in red and sidechains in blue) and a BP molecule (in yellow and green).

Molecular Dynamics Simulation

We use coarse-grained Molecular Dynamics (MD) simulation to study the structural variations of the IDTBT polymeric membrane induced by BP additions. The model is constructed based on our earlier simulations⁴⁻⁸ and relative reference⁹. Figure S1 (a) and (b) illustrate the coarse-grained model of an IDTBT polymer (with the backbone in red and sidechains in blue) and a BP molecule (in yellow and green), respectively. In the simulation, each IDTBT chain is coarse-grained as a grafted chain of a series of conjunctive spherical beads. We set the polymerization degree of the IDTBT chain as $n = 30$ and the sidechain as 4 connected beads. Additionally, each BP molecule is coarse-grained as a short chain consisting of 6 beads. For simplicity, the diameters of all the aforementioned beads are fixed as $\sigma = 1.0$, which corresponds to 4 Å. We account for the van der Waals interactions between these beads through the Lennard-Jones (LJ) potential,

$$U_{\text{LJ}}(r) = \begin{cases} 4\varepsilon \left[\left(\frac{\sigma}{r} \right)^{12} - \left(\frac{\sigma}{r} \right)^6 + S \right], & r \leq r_c \\ 0, & r > r_c \end{cases} \quad \text{S(1)}$$

where the energetic parameter is varied as $\varepsilon = 1.0 \sim 5.0$ (corresponding to $1.0 \sim 5.0 k_{\text{B}}T$ at $T = 298$ K) and the cutoff is adjusted as $r_c = 2^{1/6}\sigma \sim 2.0\sigma$ to model the volume-excluded effects and affinities between different species, as well as the crosslinking

effects of BP molecules. The LJ potential is shifted to 0 at r_c by S , and we use $\varepsilon_0 = 1.0$ (corresponding to $k_B T$ at $T = 298$ K) and $\sigma = 1.0$ (corresponding to 4 Å) as the energy and length units, respectively. We use the harmonic bond potential to model the bonding interactions between the connected beads,

$$U_{\text{Bond}} = k_b (r - r_0)^2 \quad (2)$$

where $k_b = 100 \varepsilon_0 / \sigma^2$ indicates the bond energy parameter and $r_0 = 1.0 \sigma$ is the equilibrated bond length. Further, the harmonic angle potential is used to account for chain rigidity of the IDTBT backbones,

$$U_{\text{Angle}}(\theta) = \kappa_a (\theta - \theta_0)^2 \quad (3)$$

where θ denotes the angle of the connective beads ($i-1$, i and $i+1$), θ_0 is fixed as 180° and $\kappa_a = 10$.

All simulations are performed in the canonical (NVT) ensemble via the Large-scale Atomic/Molecular Massively Parallel Simulator (LAMMPS) software package¹⁰. The 3D periodic boundary conditions are applied in the simulations. The integration MD time step is set as $t = 0.005$ (corresponding to 10 fs) and the Langevin thermostat is used to control the system temperature. For the case without BP addition, we put 25 IDTBT chains in a cubic simulation box; whereas for the cases with BP addition, we put 25 IDTBT chains and 100 BP molecules in the cubic simulation box, of which the ratio is consistent with the case of our experiments. The sizes of the simulation box are adjusted, so that the number density of the beads is controlled as 0.85. We first perform the simulations for 10^6 MD steps for equilibration and further perform another 10^6 MD steps as the production runs. To explore the effect of BP on structural variations of the polymers, we selected the ratio of crosslinking BP molecules as $f_c = 0\%$, 20%, 40%, 60%, 80% and 100%, in which the selected BP molecules show typical crosslinking effects among the sidechains of IDTBT. For each condition, we conduct dozens of parallel simulations with different initial configurations and obtain the final results through statical samplings.

Table S6. The elastic modulus and fracture strain of pristine, 1%, 2% and 3% films. The data were obtained from five samples.

Sample	Elastic modulus (E/MPa)	Fracture strain (ϵ /%)
Pristine	145±29	38±11
1%	163±37	50±6
2%	158±28	63±7
3%	193±36	53±4

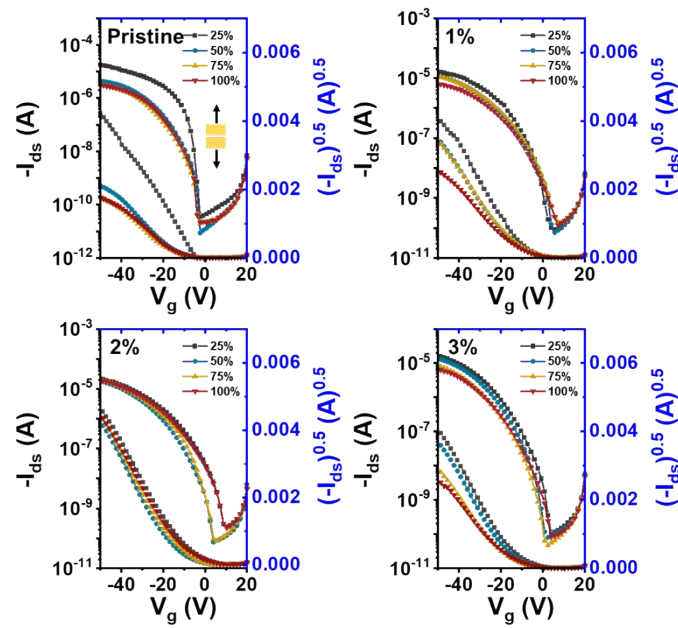


Figure S10. The transfer curves of the OFET devices fabricated from different IDTBT films (pristine, 1%, 2%, and 3%) under different strains (25%, 50%, 75%, and 100%). The stretching direction is parallel to the direction of charge carrier transport between the source and drain electrodes.

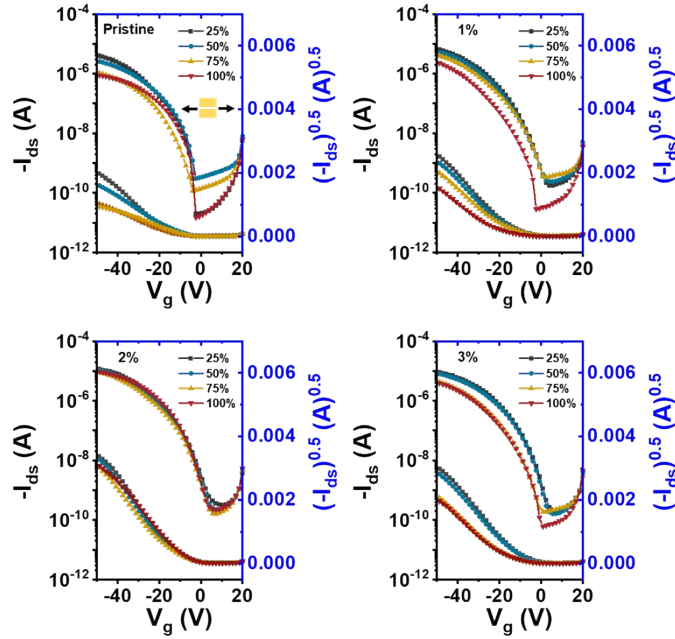


Figure S11. The transfer curves of the OFET devices fabricated from different IDTBT films (pristine, 1%, 2%, and 3%) under different strains (25%, 50%, 75%, and 100%). The stretching direction is perpendicular to the direction of charge carrier transport between the source and drain electrodes.

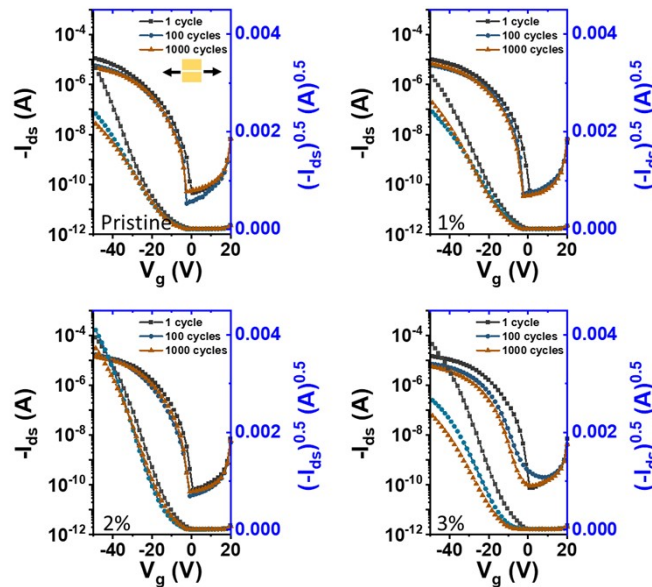


Figure S12. Transfer curves of OFET devices prepared after cyclic stretching of different films at 30% strain. The stretching direction is perpendicular to the direction of charge carrier transport between the source and drain electrodes.

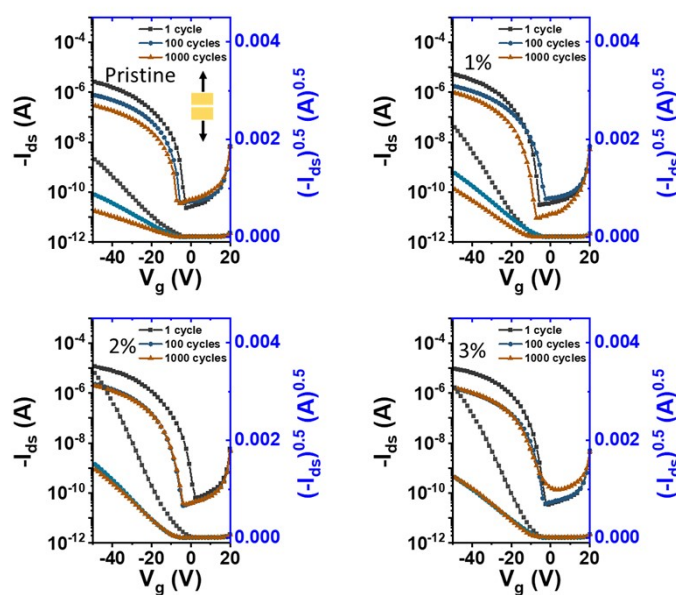


Figure S13. Transfer curves of OFET devices prepared after cyclic stretching of different films at 30% strain. The stretching direction is parallel to the direction of charge carrier transport between the source and drain electrodes.

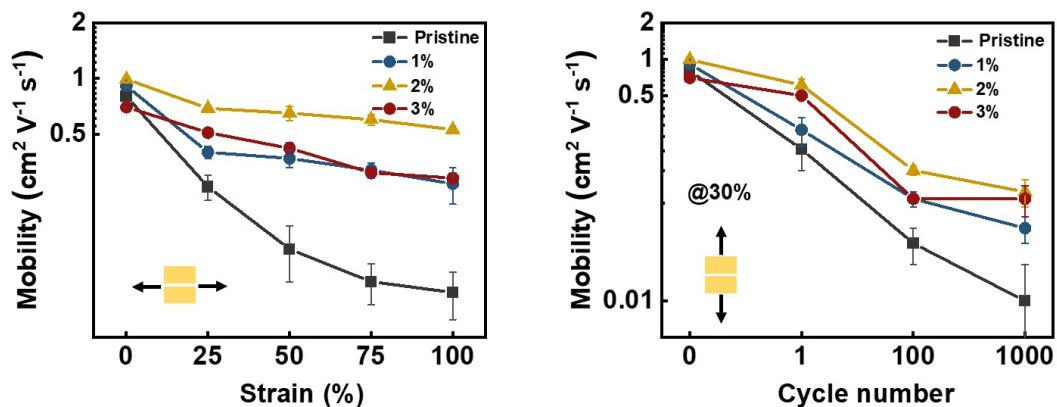


Figure S14. Changes in carrier mobility after uniaxial (left) and cyclic stretching (right).

Table S7. BGTC OFET parameters of different IDTBT films: Each set of saturation mobility (μ_{sat}) (both the average and maximum), threshold voltage (V_{th}), and $I_{\text{on}}/I_{\text{off}}$ ratio

data were extracted from five transistors with $L = 200 \mu\text{m}$ and $W = 1000 \mu\text{m}$ (parallel direction for uniaxial stretching and perpendicular direction for cyclic stretching).

Samples	μ ($\text{cm}^2 \text{V}^{-1} \text{s}^{-1}$)	$I_{\text{on}}/I_{\text{off}}$ (10^5)	V_{th} (V)	μ_{max} ($\text{cm}^2 \text{V}^{-1} \text{s}^{-1}$)	
Pristine	0%	0.80±0.10	1.41±0.51	-10.59±1.93	0.88
	25% //	0.77±0.08	5.09±0.98	-13.62±0.89	0.86
	50% //	0.29±0.04	4.15±0.70	-13.78±0.47	0.34
	75% //	0.23±0.02	1.84±0.93	-13.67±0.66	0.26
	100% //	0.24±0.02	1.11±0.28	-13.08±1.39	0.27
	30%-1 \perp	0.41±0.12	2.31±0.78	-14.02±2.66	0.55
	30%-100 \perp	0.34±0.10	2.65±1.06	-12.62±1.20	0.45
	30%-1000 \perp	0.25±0.05	0.82±0.45	-9.72±1.45	0.30
1%	0%	0.91±0.05	1.09±0.33	-1.42±2.25	0.99
	25% //	0.97±0.04	2.77±0.60	-9.44±0.51	1.02
	50% //	0.71±0.08	1.68±0.05	-12.94±0.20	0.82
	75% //	0.63±0.11	1.19±0.49	-13.06±1.51	0.72
	100% //	0.49±0.06	0.61±0.13	-6.91±4.14	0.55
	30%-1 \perp	0.60±0.03	3.34±0.98	-9.40±0.52	0.62
	30%-100 \perp	0.40±0.11	3.46±1.75	-9.90±1.71	0.58
	30%-1000 \perp	0.34±0.03	1.37±1.08	-10.82±0.57	0.38
2%	0%	0.99±0.03	0.51±0.02	-7.07±0.41	1.04
	25% //	1.04±0.06	0.85±0.04	-8.16±0.25	1.10
	50% //	1.04±0.05	2.24±0.29	-13.1±1.33	1.11
	75% //	1.05±0.05	2.46±0.20	-8.04±3.71	1.11

	100% //	0.92±0.03	0.86±0.02	-9.26±0.36	0.95
	30%-1 ⊥	0.97±0.13	2.93±1.31	-7.36±2.27	1.08
	30%-100 ⊥	0.96±0.10	4.06±0.73	-12.16±1.23	1.10
	30%-1000 ⊥	0.86±0.04	2.18±1.27	-8.80±1.92	0.92
	0%	0.70±0.01	0.69±0.04	-8.36±0.13	0.71
	25% //	0.95±0.16	1.47±0.16	-12.92±1.95	1.10
	50% //	0.97±0.15	1.77±0.20	-14.90±0.59	1.15
	75% //	0.62±0.11	1.52±0.09	-15.96±0.75	0.75
3%	100% //	0.50±0.07	0.82±0.11	-15.08±0.74	0.58
	30%-1 ⊥	0.86±0.14	2.16±0.41	-6.78±1.15	1.02
	30%-100 ⊥	0.53±0.03	0.38±0.03	-10.98±1.54	0.56
	30%-1000 ⊥	0.53±0.07	0.66±0.14	-12.58±1.25	0.63

Table S8. BGTC OFET parameters of different IDTBT films: Each set of saturation mobility (μ_{sat}) (both the average and maximum), threshold voltage (V_{th}), and $I_{\text{on}}/I_{\text{off}}$ ratio data were extracted from five transistors with $L = 200 \mu\text{m}$ and $W = 1000 \mu\text{m}$ (perpendicular direction for uniaxial stretching and parallel direction for cyclic stretching).

Samples	μ ($\text{cm}^2 \text{V}^{-1} \text{s}^{-1}$)	$I_{\text{on}}/I_{\text{off}}$ (10^5)	V_{th} (V)	μ_{max} ($\text{cm}^2 \text{V}^{-1} \text{s}^{-1}$)	
	0%	0.80±0.10	1.41±0.51	-10.59±1.93	0.88
Pristine	25% ⊥	0.26±0.04	1.87±0.63	-13.98±2.34	0.30
	50% ⊥	0.12±0.04	0.27±0.22	-15.45±4.00	0.17
	75% ⊥	0.08±0.02	1.04±0.18	-14.52±4.24	0.11

	100% ⊥	0.07±0.02	0.46±0.15	-7.77±0.80	0.09
	30%-1 //	0.18±0.06	0.96±0.42	-11.84±1.41	0.27
	30%-100 //	0.03±0.01	0.26±0.16	-6.64±1.77	0.03
	30%-1000 //	0.01±0.00	0.91±0.69	-6.57±3.54	0.02
	0%	0.91±0.05	1.09±0.33	-1.42±2.25	0.99
	25% ⊥	0.40±0.03	0.33±0.04	-13.85±0.49	0.43
	50% ⊥	0.37±0.04	0.24±0.02	-14.94±1.47	0.43
	75% ⊥	0.32±0.03	0.12±0.00	-14.41±0.95	0.34
1%	100% ⊥	0.27±0.06	1.01±0.19	-15.69±3.01	0.34
	30%-1 //	0.26±0.07	1.22±0.56	-12.72±3.19	0.32
	30%-100 //	0.07±0.01	0.44±0.32	-2.29±5.62	0.08
	30%-1000 //	0.04±0.01	0.32±0.02	-7.38±0.70	0.05
	0%	0.99±0.03	0.51±0.02	-7.07±0.41	1.04
	25% ⊥	0.69±0.02	0.36±0.03	-10.44±0.51	0.71
	50% ⊥	0.65±0.06	0.49±0.03	-11.43±0.13	0.72
	75% ⊥	0.60±0.04	0.59±0.04	-12.33±0.74	0.65
2%	100% ⊥	0.53±0.01	0.49±0.04	-8.09±0.58	0.54
	30%-1 //	0.61±0.07	1.78±0.26	-8.48±0.59	0.69
	30%-100 //	0.12±0.01	0.66±0.06	-10.44±0.37	0.13
	30%-1000 //	0.08±0.02	0.52±0.09	-9.36±0.41	0.10
	0%	0.70±0.01	0.69±0.04	-8.36±0.13	0.71
	25% ⊥	0.51±0.02	0.45±0.02	-9.75±0.31	0.54
	50% ⊥	0.42±0.03	0.47±0.02	-10.50±0.40	0.46
3%	75% ⊥	0.31±0.01	0.23±0.02	-16.28±0.81	0.32

100% \perp	0.29±0.02	0.71±0.05	-17.98±1.06	0.31
30%-1 //	0.50±0.04	2.68±0.16	-9.90±0.95	0.55
30%-100 //	0.07±0.00	0.35±0.09	-6.18±1.24	0.07
30%-1000 //	0.07±0.02	0.10±0.01	-7.22±2.46	0.08

Table S9. Charge mobilities of IDTBT films under strain in the previous literature.

M_w /PDI	Device geometries	Crack-onset strain (%)	Fracture strain (%)	Mobility before stretching ($\text{cm}^2 \text{V}^{-1} \text{s}^{-1}$)	Mobility under strain ($\text{cm}^2 \text{V}^{-1} \text{s}^{-1}$)	Reference
291 kDa/2.8 iRUM-IDTBT	BGTC	>100%	-	1.6	~1.5 (50% //)	Nature Communications, 2021, 12(1): 1-11.
295 kDa/2.7	BGTC	>100%	22	1.8	~0.6 (100% //)	Advanced Functional Materials, 2019, 29(46): 1905340.
340 kDa/3.0	BGBC	>100%	-	1.8	~0.9 (100% //)	Journal of Materials Chemistry C, 2020, 8(44): 15646-15654.
1049 kDa/3.1	TGBC	>100%	24	2.2	~0.02 (100% //)	Macromolecules, 2021, 54(21): 9896-9905.
340 kDa/3.04 IDTBT/SEBS	BGTC	>100%	326	0.7	0.6 (100% //)	Macromolecules, 2021, 55(1): 297-308.
180kDa/2.25 IDTBT/1-NIPS crosslinked	BGBC	80%	18	0.4	~0.4 (80% //)	Advanced Functional Materials, 2023,

References

1. Yutaka Ito, A. A. V., Stefan Mannsfeld, Joon Hak Oh, Michael Toney, Jason Locklin, Zhenan Bao, Crystalline Ultrasooth Self-Assembled Monolayers of Alkylsilanes for Organic Field-Effect Transistors. *J. AM. CHEM. SOC.* **2009**, *131*, 9396-9404.
2. Root, S. E.; Savagatrup, S.; Printz, A. D.; Rodriguez, D.; Lipomi, D. J., Mechanical Properties of Organic Semiconductors for Stretchable, Highly Flexible, and Mechanically Robust Electronics. *Chemical Reviews* **2017**, *117*, 6467-6499.
3. Rodriguez, D.; Kim, J.-H.; Root, S. E.; Fei, Z.; Boufflet, P.; Heeney, M.; Kim, T.-S.; Lipomi, D. J., Comparison of Methods for Determining the Mechanical Properties of Semiconducting Polymer Films for Stretchable Electronics. *ACS Applied Materials & Interfaces* **2017**, *9*, 8855-8862.
4. Wang, Z.-D.; Liang, S.; Yang, Y.; Liu, Z.-N.; Duan, X.; Li, X.; Liu, T.; Zang, H.-Y., Complex phase transitions and phase engineering in the aqueous solution of an isopolyoxometalate cluster. *Nature Communications* **2023**, *14* (1), 2767.
5. Yao, L.; Lin, C.; Duan, X.; Ming, X.; Chen, Z.; Zhu, H.; Zhu, S.; Zhang, Q., Autonomous underwater adhesion driven by water-induced interfacial rearrangement. *Nature Communications* **2023**, *14*, 6563.
6. Liu, B.; Hu, B.; Du, J.; Cheng, D.; Zang, H. Y.; Ge, X.; Tan, H.; Wang, Y.; Duan, X.; Jin, Z., Precise Molecular - Level Modification of Nafion with Bismuth

Oxide Clusters for High - performance Proton - Exchange Membranes. *Angewandte Chemie* **2021**, *133* (11), 6141-6150.

7. Zhu, Z.; Duan, X.; Li, Q.; Wu, R.; Wang, Y.; Li, B., Low-noise nanopore enables in-situ and label-free tracking of a trigger-induced DNA molecular machine at the single-molecular level. *Journal of the American Chemical Society* **2020**, *142* (9), 4481-4492.

8. Li, B.; Duan, X.; Cheng, D. M.; Chen, X. Y.; Gao, Z. X.; Ren, W. B.; Shao, K. Z.; Zang, H. Y., Controllable Transition Metal-Directed Assembly of [Mo₂O₂S₂]²⁺ Building Blocks into Smart Molecular Humidity-Responsive Actuators. *Journal of the American Chemical Society* **2022**, *145*, 2243-2251.

9. Marrink, S. J.; Risselada, H. J.; Yefimov, S.; Peter, T. D.; de Vries, A. H., The MARTINI Force Field: Coarse Grained Model for Biomolecular Simulations. *J. Phys. Chem. B* **2007**, *111*, 7812-7824.

10. Plimpton, S., Fast Parallel Algorithms for Short-Range Molecular-Dynamics. *Journal of Computational Physics* **1995**, *117* (1), 1-19.